Electron Structure of Iron Chalcogenide Clusters {Fe_3Q} from AIM and ELF Data: Effect of Hydrogen Atoms on Interatomic Interactions

Maxim R. Rizhikov,[†] Svetlana G. Kozlova,*[,†,‡,§] and Sergei N. Konchenko[†,‡]

Nikolayev Institute of Inorganic Chemistry, Russian Academy of Sciences, av. Lavrentyeva, 3, 630090 Novosibirsk, Russian Federation; Novosibirsk State University, av. Pirogova, 2, 630090 Novosibirsk, Russian Federation; and Boreskov Institute of Catalysis, Russian Academy of Sciences, av. Lavrentyeva, 5, 630090 Novosibirsk, Russian Federation

Received: July 06, 2008; Revised Manuscript Received: October 23, 2008

The electronic structure of $[Fe_3(\mu_3\text{-}Q)(CO)_9]^{2-}$ and $[(\mu\text{-}H)_2Fe_3(\mu_3\text{-}Q)(CO)_9]$ (Q = S, Se, and Te) complexes is studied with topological methods AIM and ELF. Fe−Fe bonds in $[(\mu\text{-}H)_2Fe_3(\mu_3\text{-}Q)(CO)_9]$ complexes are shown to break down in the presence of H atoms.

Introduction

Transition metal clusters with incorporated main group elements are good building blocks for "step-by-step assembling strategies" useful to design large heteronuclear cluster aggregates from fragments of lower nuclearity.[1−3] The large cluster aggregates are interesting because of their potentiality to serve as precursors for different functional materials with well-determined composition and unusual structure, especially high-ordered heterometallic nanoparticles prospective for creation of novel magnetic storage devices possessing high recording density.[4]

The iron chalcogenide clusters $[Fe_3(\mu_3\text{-}Q)(CO)_9]^{2-}$ (**1a**−**c**) and $[(\mu\text{-}H)_2Fe_3(\mu_3\text{-}Q)(CO)_9]$ (**2a**−**c**) represent an area of cluster chemistry which is rather developed regarding the molecular design of heteronuclear derivatives. Some examples of the **1a**−**c** and **2a**−**c** chemistry are shown in Scheme 1.[5−9]

The chemistry of **1a**−**c** is mainly represented by addition of different kinds of electrophiles to the clusters whose framework remains entire or undergoes slight modifications, e.g., cleavage of one M−M bond. At the same time, the known reactions of **2a**−**c** are represented predominantly by "metal substitution": degradation of the initial cluster core in the presence of appropriate organometallic complexes leading to formation of more thermally stable heteronuclear derivatives.

The numerous experimental data obtained in this area allow us to notice the following regularities in the reactivity of the clusters:

1. A framework of **1a**−**c** seems to be more stable than that of **2a**−**c**.

2. The addition of electrophiles to **1a**−**c** proceeds primarily via attachment to the Fe atoms. The chalcogenide atom plays a secondary role.

3. Addition of CH_3^+ to the S atom of **1a** is the only known example of electrophilic addition purely to chalcogenide atom. For Se and Te such examples are unknown.

To realize the regularities, the empirical data must be supplied with a profound theoretical description of their electronic structure. This work starts quantum chemical study focused on interrelationships between electronic structures of **1a**−**c** and **2a**−**c** and their reactivity.

Computational and Experimental Details

The electronic structures of the model systems **1a**−**c** (C_{3v} point group symmetry) and **2a**−**c** (C_1 point group symmetry) were calculated with the DFT method using ADF2006 code.[10] The attention was focused on studying of interactions between atoms Fe−Fe, Fe−Q, and Fe−H inside the cluster frameworks $\{Fe_3(\mu_3\text{-}Q)\}$ and $\{(\mu\text{-}H_2)Fe_3(\mu_3\text{-}Q)\}$. Basis sets consisted of Slater relativistic functions (TZP) with frozen cores chosen for Fe 2p, Te 4p, Se 3p, S 2p. We used zero order regular approximation (ZORA) to account for relativistic scalar effects together with two density functionals BLYP and BP86 to test the stability of the solutions.[11−14] The full geometry optimizations of the ground states were performed with the quasi-Newtonian method.[15] The electronic bonding energies of model systems **1a**−**c** and **2a**−**c** were calculated according to the formal reactions $3Fe + Q + 9C + 9O + 2e^- \rightarrow [Fe_3Q(CO)_9]^{2-}$ and $3Fe + Q + 9C + 9O + 2H \rightarrow [H_2Fe_3Q(CO)_9]$, where Q = S, Se, and Te, as reported in ref 16. The electron density was analyzed with topological methods of quantum chemistry based on Bader's theory of atoms in molecules and the electron localization function (ELF).[17−20]

According to the AIM method of quantum theory, the structure of a many-electron system is completely determined by the set of the critical points of electron density $\rho(r,R)$ (r and R are the coordinates of electrons and nuclei), at which the electron density gradient $\nabla^2\rho(r,R)$ is zero. The second derivatives calculated at these points form a real symmetric matrix sized 3 × 3. The chief components of this matrix determine the rank p and the signature q of the critical point $\{p,q\}$, where the rank is the number of nonzero eigenvalues, and q is the algebraic sum of their signs. For no degenerate states with $p = 3$, only four types of the critical point of electron density are possible. These are as follows: (3,−3) or nuclei critical (nc) point is the local maximum that corresponds to the positions of nuclei; (3,−1) or bond critical (bc) point is the binding saddle point characterized by the charge concentrated in one directions and decreased in two directions; (3,1) or ring critical (rc) point is the circular saddle point characterized by the charge increasing in two directions and decreasing in the third direction; and (3,3) or cage critical (cc) point is the local minimum that appears at

* Corresponding author. Tel.: (383)3307531. E-mail: sgk@che.nsk.su.
† Nikolayev Institute of Inorganic Chemistry, Russian Academy of Sciences.
‡ Novosibirsk State University.
§ Boreskov Institute of Catalysis, Russian Academy of Sciences.

10.1021/jp805941n CCC: $40.75
Published on Web 12/02/2008

TABLE 1: Interatomic Distances (Å): Calculated BLYP/BP86/Experimental[a] and Bonding Energies (ΔE, eV) of the $[Fe_3(\mu_3\text{-}Q)(CO)_9]^{2-}$ (1a−c) and $[(\mu_3\text{-}H)_2Fe_3(\mu_3\text{-}Q)(CO)_9]$ (2a−c) Complexes (Q = S (a), Se (b), Te (c))

	Fe−Fe, Å	Fe−Fe, Å	Fe−Q, Å	Fe−Q, Å	Fe−H, Å	Fe−H, Å	ΔE (BLYP/BP86)
1a	2.72/2.65/2.59	2.72/2.65/2.59	2.27/2.24/2.20	2.27/2.24/2.20	−	−	−164.3/−172.2
1b	2.76/2.69/2.62	2.76/2.69/2.62	2.43/2.39/2.30	2.43/2.39/2.30	−	−	−163.5/−171.4
1c	2.81/2.70/2.63	2.81/2.70/2.63	2.63/2.60/2.49	2.63/2.60/2.49	−	−	−162.6/−170.5
	Fe1−Fe2, Å	Fe2−Fe2, Å	Fe1−Q, Å	Fe2−Q, Å	Fe1−H, Å	Fe2−H, Å	ΔE (BLYP/BP86)
2a	2.78/3.03/2.66	2.69/2.81/2.60	2.31/2.33/2.22	2.27/2.29/2.19	1.68/1.81/1.55	1.71/1.67/1.67	−168.6/−177.6
2b	2.80/3.09/2.69	2.71/2.81/2.61	2.46/2.47/2.34	2.43/2.43/2.31	1.67/1.83/1.58	1.71/1.66/1.66	−167.8/−177.0
2c	2.86/3.16/2.70	2.73/2.88/2.67	2.68/2.67/2.51	2.64/2.63/2.48	1.67/1.85/1.49	1.70/1.66/1.68	−166.9/−176.3

[a] Average values for corresponding bonds are given in the cases when the distances were measured few times (**1a**,[7a,20] **1b**,[21] **1c**,[23] **2a**,[7a] **2b**,[23] **2c**[23]).

SCHEME 1: Reactivity of $[Fe_3(\mu_3\text{-}Q)(CO)_9]^{2-}$ (Q = S (1a), Se (1b), Te (1c)) and $[(\mu\text{-}H)_2Fe_3(\mu_3194Q)(CO)_9]$ (Q = S (2a), Se (2b), Te (2c)) toward Some Electrophilic Agents and Organometallic Complexes: (i) $RECl_2$ (E = P, As, Sb, Bi);[5] (ii) $[L_nM]^{2+}$ (M = Rh, Ir, Pt, Mn);[6] (iii) $(CH_3)_3O^+$, Q = S; (iv) $(CH_3)_3O^+$, Q = Se, Te;[7] (v) $[Cp^xM(CO)_3]_2$ (M = Mo, W; $Cp^x = C_5H_5$, C_5Me_5);[8] (vi) $[Cp^xMo(CO)_3]_2$ (M = W; M′ = Mo);[8] (vii) $[Co_2(CO)_8]$; (viii) $[CpMo(CO)_3AsMe_2]$ (M = Co, M′ = Mo)[9]

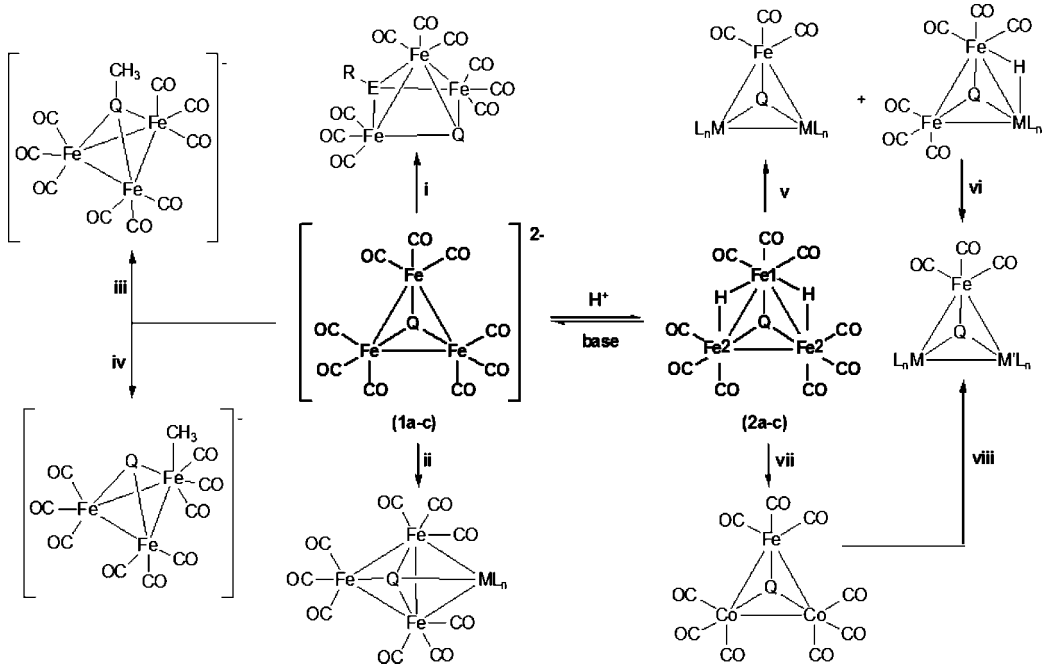

those points where the electron density increases in all three directions. The number and type of critical points in a molecule or molecular complex is defined by the Poincar−Hopf equation, nc − bc + rc − cc = 1. The numerical values of the parameters of the critical points such as the electron density $\rho(r,R)$, the Laplacian of electron density $\nabla^2\rho(r,R)$, the density ratio between the kinetic energy G, and the potential energy U of electrons at the critical point determine the character of interatomic interactions (covalence, ionicity, metallicity, etc.).

TABLE 2: Calculated Atomic Charges in the $[Fe_3(\mu_3\text{-}Q)(CO)_9]^{2-}$ (1a−c) and the $[(\mu_3\text{-}H)_2Fe_3(\mu_3\text{-}Q)(CO)_9]$ (2a−c) Complexes (in Electron Charge Units, e) (Q = S (a), Se (b), Te (c))

1	Fe	Fe	Fe	Q		
a	−0.088	−0.088	−0.088	−0.146	−	−
b	−0.096	−0.096	−0.096	−0.114	−	−
c	−0.107	−0.107	−0.107	−0.061	−	−

2	Fe2	Fe1	Fe2	Q	H	H
a	−0.033	−0.007	−0.033	−0.004	−0.058	−0.058
b	−0.042	−0.017	−0.042	0.065	−0.061	−0.061
c	−0.057	−0.029	−0.057	0.174	−0.065	−0.065

Another approach to electron density analysis is implemented in the ELF method. In this method, we analyze the function of the form

$$\mathrm{ELF}(\vec{r}) = \frac{1}{1+\left(\frac{D(\vec{r})}{D_h(\vec{r})}\right)^2}$$

where

$$D(\vec{r}) = \frac{1}{2}\sum_{j=1}^{N}\nabla\varphi_j(\vec{r})^2 - \frac{1}{8}\frac{|\nabla\rho(\vec{r})|^2}{\rho(\vec{r})}$$

$$D_h(\vec{r}) = \frac{3}{10}(3\pi^2)^{2/3}\rho(\vec{r})^{5/3}$$

$$\rho(\vec{r}) = \sum_{j=1}^{N}|\varphi_j(\vec{r})|^2$$

Summation of j is done over all $N\varphi_j$ molecular orbitals; $\rho(\mathbf{r})$ is

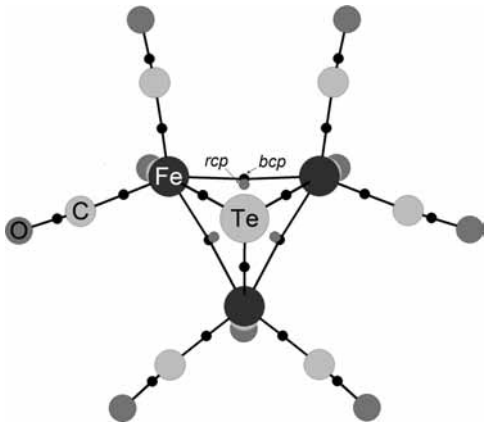

Figure 1. Critical point in the $[Fe_3(\mu_3\text{-Te})(CO)_9]^{2-}$ (**1c**) anion.

TABLE 3: Electron Density ρ (e/bohr^3), Laplacian of the Electron Density $\nabla^2\rho$ (e/bohr), and Kinetic (G) and Potential (U) Energy Densities (hartrees/bohr^3) in the Critical Points in the Cluster Cores of $[Fe_3(\mu_3\text{-Q})(CO)_9]^{2-}$ (1a−c) Complexes (Q = S (a), Se (b), Te (c))[a]

	fragments	critical point	ρ	$\nabla^2\rho$	$G(x)$	$U(x)$
1a	Fe−S	bc	0.069	0.141	0.054	−0.072
1b	Fe−Se	bc	0.063	0.110	0.044	−0.060
1c	Fe−Fe (3)	bc	0.031	0.018	0.013	−0.022
	Fe−Te (3)	bc	0.051	0.090	0.028	−0.034
	Fe−Te−Fe (3)	rc	0.034	0.049	0.016	−0.020

[a] Numbers in parentheses signify the number of critical points.

TABLE 4: Geometric Properties of Fe−E bc Points in $[Fe_3(\mu_3\text{-Q})(CO)_9]^{2-}$ (1a−c, E = Fe, Q) Complexes (Q = S (a), Se (b), Te (c))

	bond	Fe−bc, Å	bc−E, Å	∠Fe−bc−E, deg
1a	Fe−S	1.096	1.243	179.01
1b	Fe−Se	1.121	1.311	179.02
1c	Fe−Fe	1.394	1.394	172.43
	Fe−Te	1.187	1.435	179.01

the electron density; $D_h(r)$ is the density of the Thomas−Fermi kinetic energy for the homogeneous electron gas, which acts as a normalizing multiplier; $D(r)$ is interpreted as excess density of the local kinetic energy of electrons (fermions) resulting from repulsion according to the Pauli principle relative to the density of the local kinetic energy of bosons. In its final formulation, the ELF defines the boson behavior of electron density. The ELF is assumed to approximate 1 in regions of space that are typical of the maximum localization of electron pairs with the antiparallel spins or bosons (colored blue in our drawings). The ELF is ∼0.5 in regions where the electron density is close to that of the homogeneous electron gas (green) and ∼0 in regions with delocalized electrons (red). The character of interatomic bonding can be inferred from the arrangement of the ELF basins, which consist of a set of all gradient lines of ELF that terminate at the local maximum point of the latter. Monosynaptic basins $V(X)$ are associated with the lone electron pairs; disynaptic basins $V(X1,X2)$, with the two-center bonds; polysynaptic basins $V(X1,X2,...,Xn)$, with many-center bonds.

Analysis of critical points was carried out using the Xaim software developed by Jose Carlos Ortiz and Carles Bo, Universitat Rovira i Virgili, Tarragona, Spain. ADFView program with grid step 0.05 Å was used to visualize ELF isolines.

The ^{1}H NMR spectra were recorded on a Bruker Avance 300 spectrometer (^{1}H 300.132 MHz) of the **2a−c** solutions in CD_2Cl_2, and their chemical shifts (δ, ppm) were referenced to the signals of tetramethylsilane (TMS). Besides, the ^{1}H NMR chemical shifts were computed for the fully optimized geometry of the **2a−c** model systems by the DFT-GIAO method.[21]

Results

Tables 1 and 2 show interatomic distances, bonding energies, and atomic charges for the **1a−c** and **2a−c** complexes. The calculated distances are in reasonable agreement with experimental data for crystal phases.[22−25] **2a−c** systems demonstrate longer Fe1−Fe2, Fe1−Q distances and shorter Fe2−Fe2 distances than **1a-c** systems. As is seen, Fe−Fe and Fe−Q distances, in contrast to Fe−H distances, depend on the specific chosen chalcogenide element Q. The negative values of the energies of complexes **1a−c** and **2a−c** indicate that complex formations are favorable, and the thiocomplexes are characterized by a higher stability than the selenium and tellurium complexes.

In both **2a−c** and **1a−c** complexes the atomic charges are small, which indicates the prevalence of covalent bonding in the interatomic interactions. Negatively charged complexes **1a−c** are naturally characterized by the increase of negative charge on all atoms. The charge is redistributed according to the known electronegativity properties of the atoms, e.g., the maximum negative charge is concentrated on S atoms as compared to that on Se and Te. The iron atoms are characterized by small negative charges.

The bc points between Fe−Fe and Fe−Te atoms and the rc points on the Fe−Te−Fe face were located in the **1c** model structure (Table 3, Figure 1). The number of all critical points

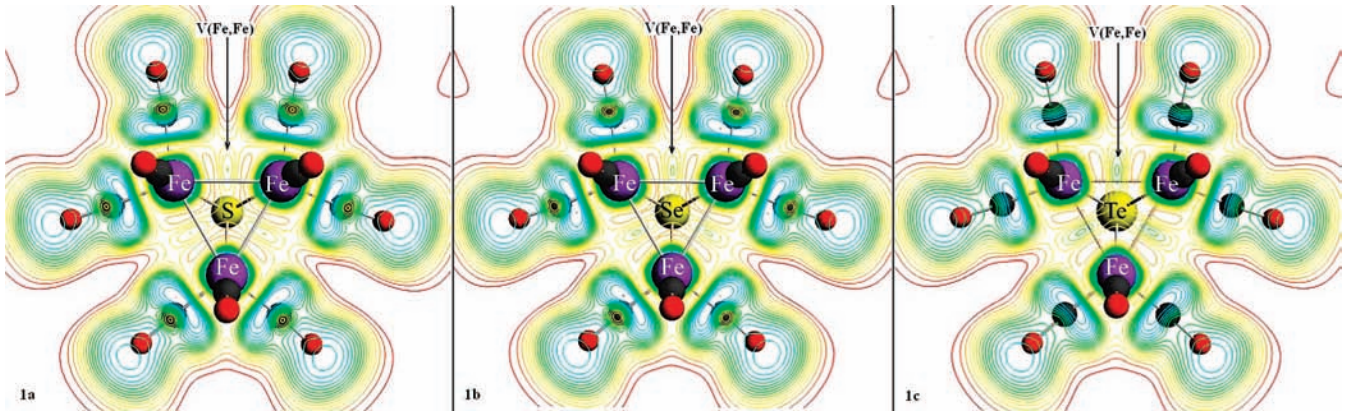

Figure 2. Fe−Fe−Fe cross-section of ELF colormap in the (**1a**), (**1b**) and (**1c**) anions. The arrows depict the V(Fe,Fe) disynaptic basins.

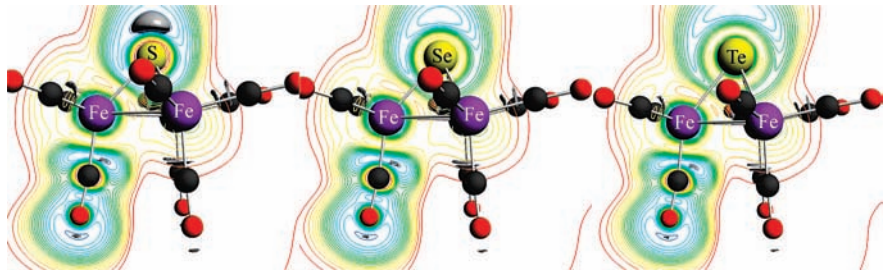

Figure 3. ELF isosurface for **1a** (left), **1b** (center), and **1c** (right) at ELF = 0.9.

TABLE 5: Electron Density ρ (e/bohr^3), Laplacian of the Electron Density $\nabla^2\rho$ (e/bohr), and Kinetic (G) and Potential (U) Energy Densities (hartrees/bohr^3) in the Critical Points in the Cluster Cores of the [(μ-H)$_2$Fe$_3$(μ_3-Q)(CO)$_9$] (2a−c) Molecules (Q = S (a), Se (b), Te (c))

		critical point	ρ	$\nabla^2\rho$	G	U
2a	Fe1−Fe2	bc	–	–	–	–
	Fe2−Fe2 (1)	bc	0.038	0.01	0.018	−0.033
	Fe1−S (1)	bc	0.067	0.111	0.046	−0.064
	Fe2−S (2)	bc	0.070	0.135	0.053	−0.072
	Fe2−H (2)	bc	0.069	0.167	0.060	−0.078
	Fe1−H (2)	bc	0.080	0.158	0.064	−0.089
	Fe1−S−Fe2−H(2)	rc	0.036	0.062	0.021	−0.026
	Fe2−S−Fe2 (1)	rc	0.038	0.055	0.022	−0.028
2b	Fe1−Fe2	bc	–	–	–	–
	Fe2−Fe2 (1)	bc	0.037	0.032	0.016	−0.024
	Fe1−Se (1)	bc	0.061	0.08	0.036	−0.052
	Fe2−Se (2)	bc	0.064	0.101	0.043	−0.06
	Fe2−H (2)	bc	0.071	0.169	0.062	−0.081
	Fe1−H (2)	bc	0.08	0.161	0.065	−0.089
	Fe1−Se−Fe2−H(2)	rc	0.034	0.056	0.019	−0.024
	Fe2−Se−Fe2 (1)	rc	0.036	0.052	0.020	−0.026
2c	Fe1−Fe2	bc	–	–	–	–
	Fe2−Fe2 (1)	bc	0.035	0.028	0.014	−0.021
	Fe1−Te (1)	bc	0.052	0.079	0.027	−0.033
	Fe2−Te (2)	bc	0.049	0.064	0.022	−0.028
	Fe2−H (2)	bc	0.073	0.190	0.068	−0.088
	Fe1−H (2)	bc	0.082	0.183	0.071	−0.097
	Fe1−Te−Fe2−H (2)	rc	0.031	0.055	0.016	−0.017
	Fe2−Te−Fe2 (1)	rc	0.034	0.049	0.016	−0.020

[a] Numbers in parentheses signify the number of critical points.

TABLE 6: Geometric Properties of Fe−E bc Points in the [(μ-H)$_2$Fe$_3$(μ_3-Q)(CO)$_9$] (2a−c) Molecules (E = Fe, Q and Q = S (a), Se (b), Te (c))

		Fe−bc, Å	bc−E, Å	∠Fe−bc−E, deg
2a	Fe2−Fe2	1.341	1.341	174.0
	Fe1− S	1.098	1.258	179.5
	Fe2− S	1.087	1.245	179.3
	Fe1−H	1.030	0.653	178.2
	Fe2−H	1.041	0.678	178.3
2b	Fe2−Fe2	1.348	1.348	176.1
	Fe1−Se	1.134	1.331	179.2
	Fe2−Se	1.119	1.313	179.0
	Fe1−H	1.027	0.648	178.1
	Fe2−H	1.039	0.672	177.9
2c	Fe2−Fe2	1.361	1.361	176.9
	Fe1−Te	1.212	1.452	178.6
	Fe2−Te	1.188	1.437	178.4
	Fe1−H	1.026	0.648	179.0
	Fe2−H	1.037	0.668	177.8

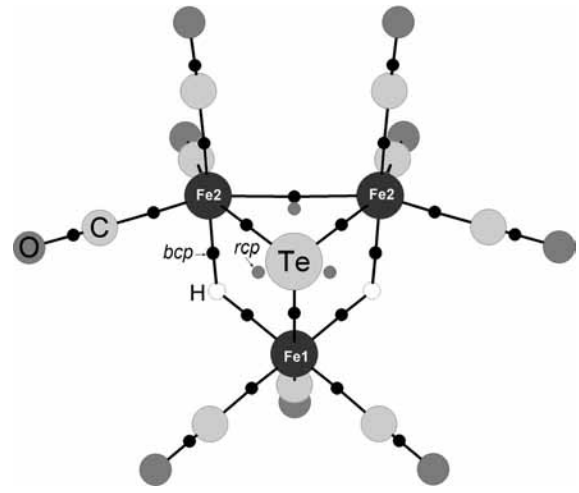

Figure 4. Critical point in the [(μ-H)$_2$Fe$_3$(μ_3-Te)(CO)$_9$] (**2c**) molecule.

obeys Poincaré−Hopf relation.[17] In **1c** the bc points are associated with small densities ρ and positive Laplacians $\nabla^2\rho$, but the density of the potential energy U does exceed the density of the kinetic energy G. It is indicative of some covalent prevalence in the considered interactions. This conclusion is also supported by ELF data which clearly image Fe−Fe interactions as disynaptic V(Fe,Fe) basins at ELF = 0.5 (Figure 2). Note that the positions of bc points ($\delta° = \angle 180° - \angle$Fe−bc−Fe ≠ 0, Table 4) and V(Fe,Fe) basins are displaced from the straight Fe−Fe line. The results prove that the Fe−Fe bonds have a bent character.

The ELF maps of **1a**−**b** structures are the same as in **1c** (Figure 2). Each complex contains three V(Fe,Fe) basins to prove

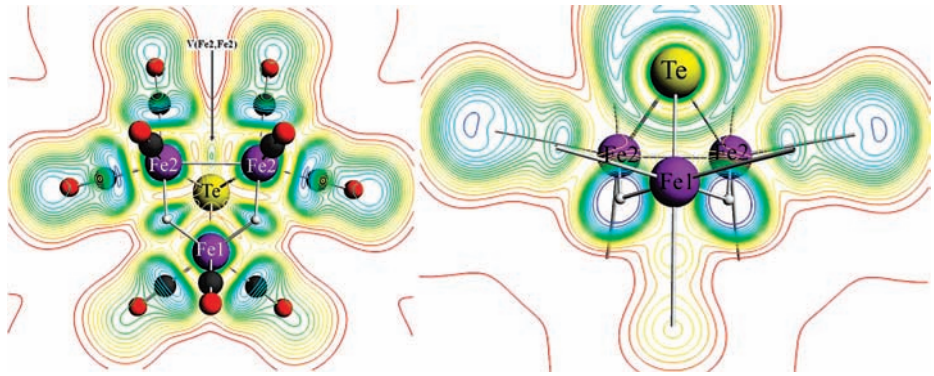

Figure 5. Fe2−Fe1−Fe2 (left) and H−Te−H (right) cross-sections of the ELF colormap in the [(μ-H)$_2$Fe$_3$(μ_3-Te)(CO)$_9$] (**2c**) molecule. The arrow depict the V(Fe2,Fe2) disynaptic basin.

unambiguously the presence of bent covalent Fe−Fe bonds. Therefore, we believe that nature of interatomic interactions in these structures should be similar to those in **1c** structure even though we could find only Fe−Q (bc) points with the Xaim program (Table 3).

The localization of the chalcogene lone pair decrease alongside (**1a**−**c**) from S to Te, i.e., the lone pair on sulfur is the most active (Figure 3).

The presence of bridge hydrogen atoms in (**2a**−**c**) molecules affects on interatomic interactions. So bc points between Fe1,2-H atoms were found, but there was no evidence of bc points between Fe1−Fe2 (the main effect). The number of critical points is the same for all (**2a**−**c**) molecules and obeys Poincaré−Hopf relation (Table 5, Figure 4). Fe2−Fe2 bonds are still characterized by the presence of disynaptic basins *V*(Fe,Fe) at ELF ∼0.5 and bc points (Table 5 and 6, Figure 5). Such disappearance of bc points between Fe atoms was discovered in the Fe$_3$(CO)$_{12}$ isomer with C_{2v} symmetry.[26] The properties of Fe−Q bonds remain almost unchanged. Fe−H interactions are classified as closed-shell according to AIM and ELF data.

The average charge concentrated on CO ligands in complexes [Fe$_3$(μ_3-Q)(CO)$_9$]$^{2-}$ is about −0.2e and is close to ∼0.0 in complexes [(μ-H)$_2$Fe$_3$(μ_3-Q)(CO)$_9$]. According to ELF and AIM data, Fe−CO interactions in the studied systems can be referred as a dative interactions similarly to those reported for Fe$_3$(CO)$_{12}$ and FeCO (Figure 3).[26,27]

The character of interaction of atoms H and Fe was analyzed with use of the data on chemical shifts ^{1}H NMR in **2a**−**c**. Computed and measured ^{1}H NMR chemical shifts in **2a**−**c** molecules show up as high negative values (Table 7). The diamagnetic component (σ^d) in **2a**−**c** is comparable to that of TMS, while the paramagnetic part (σ^p) is an order of magnitude greater. Molecular orbital's (MO) do not contain atomic shells of the hydrogen atom till HOMO-10 (highest occupied molecular orbital) and LUMO (lowest unoccupied molecular orbital). For example, HOMO and LUMO of **2a**−**c** molecules consist mainly of 3d and 3p orbitals of Fe (≥70%) (Table 8). Therefore, it may be concluded that the hydrogen's atomic shells are not directly associated with ^{1}H nuclear magnetic shielding, as it would be possible to expect at use of approaches of Ramsay theory. Most likely, high negative σ^p values are due to local magnetic fields induced by paramagnetic currents in the localization areas of Fe atoms according to the mechanism described in refs 28 and 29. The result agrees with our AIM and ELF studies about close-shell interaction between atoms of iron and hydrogen.

TABLE 7: Calculated (calc) and Measured (exp) Data of Isotropic ^{1}H NMR Chemical Shifts, and Their Diamagnetic and Paramagnetic Components (ppm)

	$\sigma_{calc}{}^d$	$\sigma_{calc}{}^p$	σ_{calc}	$\delta_{exp}{}^a$	$\delta_{calc}{}^a$
2a	29.8	20.1	49.9	−23.6 ± 0.3	−18.8
2b	29.6	20.9	50.5	−24.2 ± 0.3	−19.4
2c	30.8	20.4	51.2	−24.6 ± 0.3	−20.1

^{a} $\delta = \sigma_{TMS} - \sigma_{calc}$. Calculated absolute chemical shielding σ_{TMS} = 31.1 ppm, $\sigma_{TMS}{}^d$ = 28.3 ppm, $\sigma_{TMS}{}^p$ = 2.8 ppm.

TABLE 8: HOMO and LUMO Structure (%), Q = S (a), Se (b), Te (c)

	2a		2b		2c	
	HOMO	LUMO	HOMO	LUMO	HOMO	LUMO
Fe 3d	57.3	60.7	57.3	61.8	56.6	60.9
Fe 3p	14.6	5.8	15.0	5.9	17.4	6.2
Q np	5.3	2.1	3.9	2.8	2.3	3.4
O 2p	−	−	4.7	1.1	6.2	2.3
C 2s	4.0	11.4	5.7	12.6	5.1	12.1
C 2p	−	−	5.1	3.0	6.2	3.4
H 1s	−	−	−	1.1	−	1.3

Conclusion

The results of quantum-chemical study of [Fe$_3$(μ_3-Q)(CO)$_9$]$^{2-}$ (**1a**−**c**) and [(μ_3-H)$_2$Fe$_3$(μ_3-Q)(CO)$_9$] complexes (**2a**−**c**) can explain the experimental facts mentioned in the Introduction.

Higher stability of the anion clusters **1a**−**c** can be explained the following way: both **1a**−**c** and **2a**−**c** clusters include bent bonds Fe−Fe, Fe−Q, and Fe−H with the maximum tension between Fe−Fe ($\delta° \approx 3°-8°$). When two hydrogen atoms get coordinated to the {Fe$_3$} fragment the cycle {Fe−Q−Fe} gets broken, i.e., bc point disappears on the bent Fe−Fe bond. A new cycle {Fe−Q−Fe−H} appears with a corresponding rc point (Table 5). Such behavior of critical points can be interpreted as a break of covalent bonding between Fe atoms. The conclusion is supported by the ELF data. Therefore, the disappearance of covalent bonding between Fe atoms can lead to the lower stability of **2a**−**c** as compared to **1a**−**c**.

The negative charge on the iron atoms increases when S atom is replaced by Se and Te, and the charge on the chalcogens decreases. Therefore, the bonding of electrophilic particles with the iron atoms is quite expectable.

Among all complexes **1a**−**c**, the S atom in the **1a** complex has the maximum negative charge. Besides, the S atom demonstrates the maximum localization of the lone electron pair. This explains the how **1a** differs from **1b** and **1c** in the addition

reaction CH^{3+}. **1a** complex attaches CH^{3+} group to the chalcogen atom rather than to the iron atoms.

Acknowledgment. The study was supported by Russian Foundation for Basic Research (Grant 08-03-00826).

References and Notes

(1) Roberts, D. A.; Geoffroy, G. L. In *Comprehensive Organometallic Chemistry*; Wilkinson, C., et al., Eds.; Pergamon Press: New York, 1982; Vol. 6, p 763.

(2) Fenske, D. In *Clusters and colloids: from theory to applications*; Schmid, G., Ed.; VCH: Weinheim, Germany, 1994; p 212.

(3) Whitmire, K. H. *J. Coord. Chem.* **1988**, *17*, 95–203.

(4) Scholz, W.; Suess, D.; Schrefl, T.; Fidler, J. *J. Appl. Phys.* **2004**, *95*, 6807–6809.

(5) (a) Konchenko, S. N.; Pushkarevsky, N. A.; Virovets, A. V.; Scheer, M. *Dalton Trans.* **2003**, *4*, 581–585. (b) Pushkarevsky, N. A.; Bashirov, D. A.; Terent'eva, T. G.; Virovets, A. V.; Peresypkina, E. V.; Krautscheid, H.; Konchenko, S. N. *Koord. Khim.* **2006**, *32* (6), 416–426 (in Russian). (c) Konchenko, S. N.; Pushkarevsky, N. A.; Virovets, A. V.; Scheer, M. *Dalton Trans.* **2003**, *4*, 581–585. (d) Fischer, K.; Deck, W.; Schwarz, M.; Vahrenkamp, H. *Chem. Ber.* **1985**, *118*, 4946–4964.

(6) (a) Konchenko, S. N.; Pushkarevsky, N. A.; Scheer, M. *J. Cluster Sci.* **2003**, *14* (3), 299–312. (b) Pushkarevsky, N. A.; Konchenko, S. N.; Scheer, M. *J. Cluster Sci.* **2007**, *18* (3), 606–617. (c) Schauer, C. K.; Harris, S.; Sabat, M.; Voss, E. J.; Shriver, D. F. *Inorg. Chem.* **1995**, *34*, 5017–5028.

(7) (a) van Hal, J. W.; Whitmire, K. H. *Organometallics* **1998**, *17*, 5197–5201. (b) Cherng, J.-J.; Tsai, Y.-C.; Ueng, C.-H.; Lee, G.-H.; Peng, S.-M.; Shieh, M. *Organometallics* **1998**, *17*, 255–261.

(8) Konchenko, S. N.; Virovets, A. V.; Tkachev, S. V.; Podberezskaya, N. V.; Varnek, V. A. *J. Struct. Chem.* **1998**, *39* (5), 728–733.

(9) (a) Richter, F.; Vahrenkamp, H. *Chem. Ber.* **1982**, *115*, 3224–3242. (b) Richter, F.; Roland, E.; Vahrenkamp, H. *Chem. Ber.* **1984**, *117*, 2429–2437.

(10) Amsterdam Density Functional (ADF) program, Release 2005.02; Vrije Universteit, Amsterdam, The Netherlands, 2005.

(11) van Lenthe, E.; Ehlers, A. E.; Baerends, E. J. *J. Chem. Phys.* **1999**, *110*, 8943–8953.

(12) Becke, A. D. *Phys. Rev. A* **1988**, *38*, 3098–3100.

(13) Lee, C.; Yang, W.; Parr, R. G. *Phys. Rev. B* **1988**, *37* (2), 785–789.

(14) Perdew, J. P. *Phys. Rev. B* **1986**, *33* (12), 8822–8824.

(15) Versluis, L.; Ziegler, T. *J. Chem. Phys.* **1988**, *88*, 322–328.

(16) Bickelhaupt, F. M.; Baerends, E. J. *Rev. Comput. Chem.* **2000**, *15*, 1–86.

(17) Bader, F. *Atoms in Molecules: A Quantum Theory*; Clarendon: New York, 1990.

(18) Becke, A. D.; Edgecombe, K. E. *J. Chem. Phys.* **1990**, *92*, 5387–5403.

(19) Savin, A.; Jepsen, O.; Flad, J.; Andersen, O. K.; Preuss, H.; von Schnering, H. G. *Angew. Chem.* **1992**, *31*, 187–188.

(20) Silvi, B.; Savin, A. *Nature* **1994**, *371*, 683–686.

(21) Schreckenbach, G.; Ziegler, T. *J. Phys. Chem.* **1995**, *99*, 606–611. Te Velde, G. F.; Bickelhaupt, M.; Baerends, E. J.; Fonseca Guerra, C.; van Gisbergen, S. J. A.; Snijders, J. G.; Ziegler, T. *J. Comput. Chem.* **2001**, *22* (9), 931–967.

(22) (a) Al-Ani, F. T.; Hughes, D. L.; Pickett, C. J. *J. Organomet. Chem.* **1986**, *307* (2), 31–34. (b) Zhigui, Z.; Lixin, W.; Hengbin, Z.; Ling, Y.; Yuguo, F. *Eur. J. Solid State Inorg.Chem.* **1991**, *28*, 1269–1280.

(23) (a) Bachman, R. E.; Whitmire, K. H. *Inorg. Chem.* **1994**, *33*, 2527–2533. (b) Konchenko, S. N.; Virovets, A. V.; Varnek, V. A.; Tkachev, S. V.; Podberezskaya, N. V.; Maksakov, V. A. *J. Struct. Chem.* **1996**, *37*, 297–304. (c) Holliday, R. L.; Roof, L. C.; Hargus, B.; Smith, D. M.; Wood, P. T.; Pennington, W. T.; Kolis, J. W. *Inorg. Chem.* **1995**, *34*, 4392–4401.

(24) Roof, L. C.; Smith, D. M.; Drake, G. W.; Pennington, W. T.; Kolis, J. W. *Inorg. Chem.* **1995**, *34*, 337–345.

(25) Bachman, R. E.; Whitmire, K. H.; van Hal, J. *Organometallics* **1995**, *14*, 1792–1801.

(26) Andrés, J.; Berski, S.; Feliz, M.; Llusar, R.; Sensato, F.; Bernard Silvi, B. C. R. *Chimie* **2005**, *8*, 1400–1412.

(27) Pilme, J.; Silvi, B.; Alikhani, M. E. *J. Phys. Chem. A* **2003**, *107*, 4506–4514.

(28) Buckingham, A. D.; Stephens, P. J. *J. Chem. Soc.* **1964**, 2747–2759.

(29) Ruiz-Morales, Y.; Schreckenbach, G.; Ziegler, T. *Organometallics* **1996**, *15*, 3920–3923.

JP805941N